IEEE Access
Multidisciplinary | Rapid Review | Open Access Journal

Received August 1, 2018, accepted September 3, 2018, date of publication September 10, 2018, date of current version October 8, 2018.

Digital Object Identifier 10.1109/ACCESS.2018.2869331

Deformable Head Atlas of Chinese Adults Incorporating Inter-Subject Anatomical Variations

ZHAOFENG CHEN[1,2], TIANSHUANG QIU[1], LI HUO[3], LIJUAN YU[4], HONGCHENG SHI[5], YANJUN ZHANG[6], AND HONGKAI WANG[1], (Member, IEEE)

[1]Faculty of Electronic Information and Electrical Engineering, Dalian University of Technology, Dalian 116024, China
[2]School of Electronic Engineering, Jiujiang University, Jiujiang 332005, China
[3]Department of Nuclear Medicine, Peking Union Medical College Hospital, Beijing 100730, China
[4]The Affiliated Cancer Hospital, Hainan Medical University, Haikou 510530, China
[5]Department of Nuclear Medicine, Zhongshan Hospital, Fudan University, Shanghai 200032, China
[6]Department of Nuclear Medicine, The First Affiliated Hospital of Dalian Medical University, Dalian 116011, China

Corresponding authors: Tianshuang Qiu (qiutsh@dlut.edu.cn) and Hongkai Wang (wang.hongkai@dlut.edu.cn)

This work was supported in part by the Youth Program of the National Natural Science Foundation of China under Grant 81401475, in part by the General Program of the National Natural Science Foundation of China under Grants 61571076, 81171405, 81671771, 61139001, 61172108, 61671105, and 81241059, in part by the General Program of the Liaoning Science and Technology Project under Grant 2015020040, in part by the Cultivating Program of the Major National Natural Science Foundation of China under Grant 91546123, in part by the National Key Research and Development Program under Grant 2016YFC0106402, in part by the Science and Technology Star Project Fund of Dalian City under Grant 2016RQ019, in part by the Basic Research Funding of Dalian University of Technology under Grants DUT14RC(3)066 and DUT16RC(3)099), and in part by the Fundamental Research Funds for Central Universities under Grant DUT15LN02.

ABSTRACT To date, many digital atlases of the human head have been developed, but few incorporate the anatomical variations of the population. In this paper, for the first time, we constructed two digital head atlases (DHAs) of Chinese male and female adults, which can be deformed to simulate the inter-subject anatomical variations. The atlases were developed to assist with personalized medical treatment, population-based radio magnetic simulation, and medical imaging device design. The statistical shape model approach was used to construct the atlases based on a training set of 65 computed tomography (CT) images (including those of 46 males and 19 females). To evaluate the accuracy of anatomy modeling, we compared the atlas morphometry parameters with the reference values of the Chinese population and observed the reasonable agreement between them. Compared with the existing digital human head atlases, a unique feature of the DHA is the capability of emulating individual head anatomy via model deformation. This feature is validated by registering the DHAs to patient CT images. The registered atlases provide complete anatomy of the target subjects, including the structures that are not clearly visible in the CT images.

INDEX TERMS Deformable models, personalized anatomy modeling, statistical shape model, digital human head atlases.

I. INTRODUCTION

The human head is a complex and multifunctional structure system. Digital atlases of the human head are widely used in clinical practice and medical research, such as medical image analysis [1]–[3], surgery planning [4]–[7], anatomy-based simulation [8]–[10], radiotherapy planning [11]–[13], organ dosimetry calculation [14]–[16], and anatomy education [17]–[22]. To provide reference anatomy of the human head, many existing head atlases incorporate very fine details of the head structures. The current head atlases mostly represent anatomical shapes via polygonal meshes and, thus, are convenient for rendering and accurate for anatomical modeling. Nowinski [23], [25] and Nowinski *et al.* [24] constructed human head atlases containing intracranial vasculature, white matter tracts, cranial nerves, head muscles and glands, skull and extracranial vasculature. Mitsuhashi *et al.* [26] created human body polygon data called "BodyParts3D" including the comprehensive head anatomy, following the anatomical ontology wherein the anatomical concepts were represented by three-dimensional (3D) structure segments of an adult human male.

To the best of our knowledge, most available head atlases were developed based on only one reference subject. However, the recent development of personalized medicine has created a demand for statistical modeling of the population. To meet this requirement, Lee *et al.* [27] constructed the

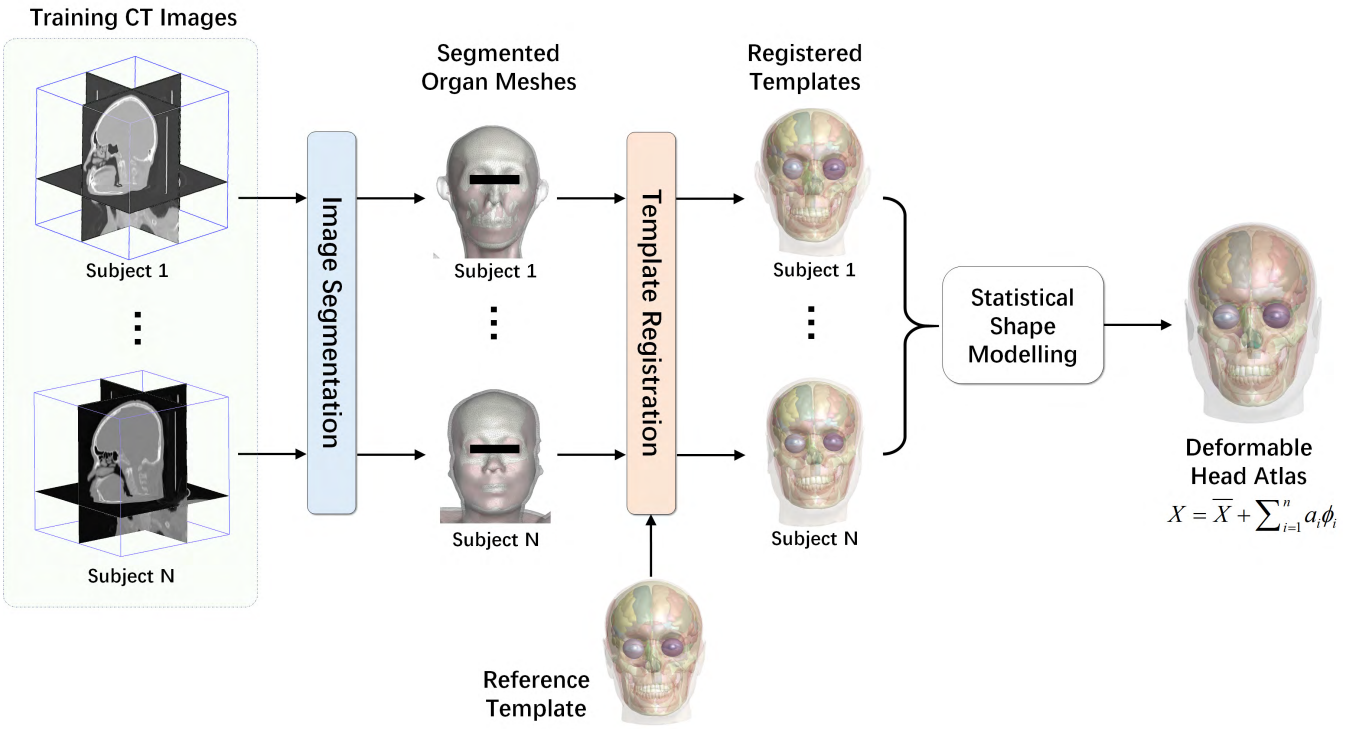

FIGURE 1. The workflow of deformable head atlas construction.

population head model (PHM) repository of 50 different head models from magnetic resonance (MR) images, but they did not perform statistical modeling of inter-subject anatomical variations. There are also many population-based human brain atlases, such as the Brain Research Through Advancing Innovative Neurotechnologies (BRAIN) Initiative [28], [29], the Human Brain Project [30], the Human Connectome Project (HCP) [31], the Allen Brain Atlas [32], and the brain atlas of anatomical and functional connections [33]. These atlases are instrumental in promoting neural science studies, but they are not for the entire human head.

To meet the requirement of whole-head personalized modeling, it is desirable to develop a deformable atlas, which incorporates realistic anatomical variations learned from medical images of real subjects. Therefore, this study develops deformable head atlases (DHAs) based on a training set of computed tomography (CT) images of healthy Chinese adults. The statistical shape model (SSM) method [34]–[37] is used to learn realistic anatomical variations from the training samples. The DHAs can be deformed to match individual head anatomies for personalized simulation and individualized medical treatment such as electromagnetic exposure simulation, plastic and aesthetic surgery, radiation therapy planning, etc.

II. METHODS

Fig. 1 illustrates the workflow of atlas construction. Head CT images of different normal subjects are segmented into anatomical regions. A template mesh model of the reference human head anatomy is registered to each segmented image, obtaining individualized anatomical representation of each subject. The statistical shape model of the head anatomy is constructed based on the registered templates of the training subjects. This workflow is used to construct a male atlas and a female atlas. The details of the workflow are explained in the following subsections.

A. TRAINING DATA COLLECTION

This study collects retrospective data of head CT images stored in the database of Chinese hospitals. The critical requirement of the training images is to present the normal anatomy of the entire head. However, clinical diagnostic CT or MR images do not meet this requirement because they mostly cover the pathological parts of patient heads. Therefore, we collect the health screening PET/CT images accumulated during the past 20 years. These images were acquired for the torso and head region, but we used only the CT images of the head and saved the PET images for future functional modeling. To ensure proper coverage of the Chinese population, the images were collected from four central hospitals in the northeast, southeast, and central areas of China. After data selection, the data of 65 asymptomatic subjects were used as training data. Table 1 shows the gender and age distributions of the selected training subjects. The acquisition parameters of the CT images were 100-140 kV of the tube voltage and 28-298 mA of current, with pixel sizes ranging from 0.59 to 1.37 mm and the inter-slice spacing ranging between 1.25 and 3.00 mm.

TABLE 1. The number of collected images of different ages and genders.

Ages	Number of Collected Images		
	Male	Female	Total
30–39	4	3	7
40–49	13	2	15
50–59	8	8	16
60–69	15	2	17
70–79	3	4	7
80–89	3	0	3
All	**46**	**19**	**65**

TABLE 2. The list of organ structures included in the atlas.

Organ System	Numbers of Organs
Head integumentary system	1
Head muscular system	69
Skull bones	50
Brain structures	99
Adipose	1
Total	**220**

B. TRAINING IMAGE SEGMENTATION

Due to the imperfect soft tissue contrast of CT imaging, only a limited number of head structures (i.e., the skin, skull, facial muscles and subcutaneous fat) could be segmented from the training images. The skin and skull were segmented via intensity thresholding, and the threshold for each image was manually adjusted to ensure accurate segmentation. The facial muscles and subcutaneous fat were separated by thresholding the region between the skin and the skull surface. A radiologist with over ten years of experience proofread and corrected the segmentation results using the MITK software [38]. Eventually, the Marching Cubes algorithm [39] was used to convert the segmented structures into triangular surface meshes, which would be used as the target meshes for the next step of template mesh registration.

C. TEMPLATE MESH REGISTRATION

To compensate for the structures that are not clearly visible in the CT images, a reference template model of the full head anatomy [40] was created for each segmented CT image. Table 2 shows the anatomical structures contained in the template model.

The registration of the template model is achieved using the landmark-based robust point-matching (RPM) method [41]. The surface points of skin, skull, facial muscles are extracted from the template model and registered to same structures segmented from the individual CT images. To ensure accurate registration, anatomical landmarks are manually specified on the surface meshes by human experts. The registration procedure produces a nonlinear thin plate spline (TPS) transform, which is used to map the complete template model to the individual image space, obtaining the mapped regions of all head structures. After template registration, each vertex of the template model is mapped to similar anatomical locations of different training subjects, and the anatomy of different training subjects is represented by the same mesh topology. It is worth noting that although the thresholding of the previous organ segmentation step does not always yield smooth edges, the registered organ template meshes has smooth surfaces and remedies the unsmooth segmentation.

D. STATISTICAL SHAPE MODEL CONSTRUCTION

The inter-subject anatomical variations are modeled using the statistical shape model (SSM) approach based on the registered templated meshes of the training subjects. First, generalized procrustes analysis (GPA) [42] was applied to normalize the training shapes, and then, the deformable atlas was constructed as a point distribution model using principal component analysis (PCA) [34]. PCA was used to first calculate the covariance matrix for the shape vectors of all training subjects and then to perform eigen decomposition of the covariance matrix. The resultant eigenvectors $\{\phi_i\}, i = 1, \cdots, n$, were the modes of shape variations, and the eigenvalues $\{\lambda_i\}, i = 1, \cdots, n$ were the corresponding variances of each mode. The shape variation modes were in order of their variance values ($i.e. \lambda_1 \geq \lambda_2 \geq \cdots \geq \lambda_n$); thus, mode 1 corresponds to the largest variance, mode 2 corresponds to the second largest variance, and so on. The variance percentage ratio of the mode i is obtained by $\lambda_i \Big/ \left(\sum_{j=1}^{n} \lambda_j\right)$.

The SSM is expressed as an average shape plus a linear combination of the different shape variation patterns:

$$X = \overline{X} + \sum_{i=1}^{n} a_i \phi_i \tag{1}$$

where X is an instance of the shape generated by the model. X is represented as a shape vector $(x_1, y_1, z_1, x_2, y_2, z_2, \cdots, x_k, y_k, z_k)^T$ containing the 3D coordinates of k mesh vertices. $\overline{X}$ is the mean shape vector of all the training subjects. $\{a_i\}, i = 1, \cdots, n$ are the shape parameters, which serve as the weights of the variation modes. Different values of $\{a_i\}$ generate different instances of the model. The continuous change in the value of $\{a_i\}$ results in continuous deformation in the model shape, resulting in real-time deformation of the head anatomy.

III. RESULTS

A. OBSERVATION OF THE ANATOMICAL VARIATION MODES

To observe the anatomical meaning of each variation mode, we separately adjusted the shape parameter a_i of each mode to see the corresponding deformation pattern. During the adjustment for each mode, the shape parameters of other modes are set to zero. The value of each a_i was adjusted within the range $[-2\sqrt{\lambda_i}, 2\sqrt{\lambda_i}]$, where λ_i is the eigenvalue of the i^{th} mode, and $[-2\sqrt{\lambda_i}, 2\sqrt{\lambda_i}]$ is the plausible range of the anatomical deformation commonly used in previous studies.

Fig. 2 shows the mean shapes of the male and female SSMs. The anatomical structures in correspondence to Table 2 are rendered with different colors. The DHAs include 218 sub-structures of the facial muscles, skull bones and brain, offering good anatomical details for potential simulation and image analysis applications.

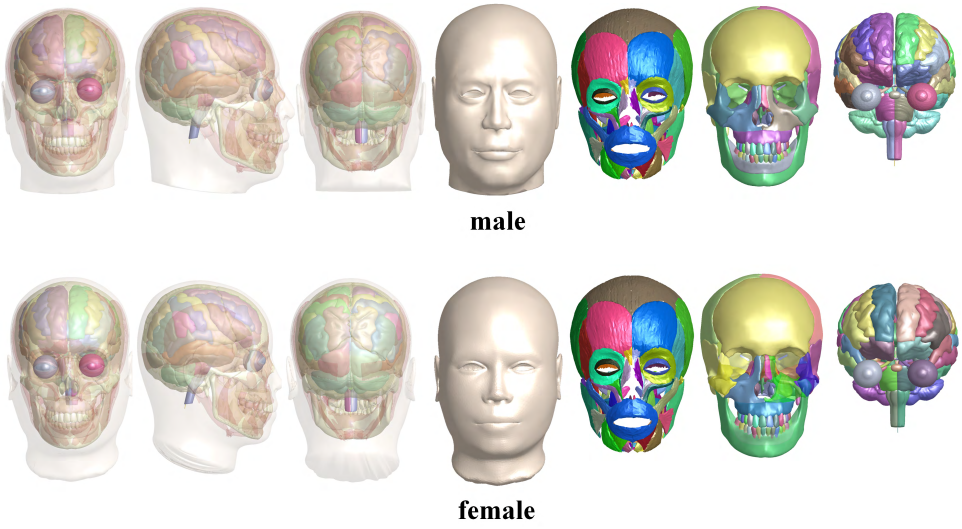

FIGURE 2. Anatomical structures contained in the male and female atlases. The first to third columns demonstrate semi-transparent rendering of all anatomical structures from different view angles. The fourth to seventh columns show the skin, muscles, skull bones and brain structures, respectively.

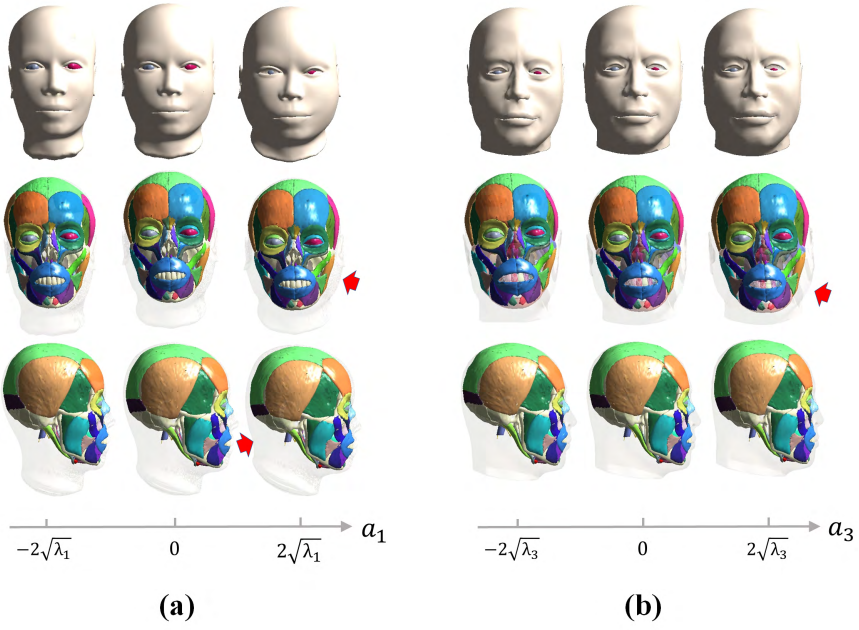

FIGURE 3. Variation modes related to fat quantity change in the female (a) and male (b) atlases. Different columns correspond to different values of the shape parameter. The top row renders the atlases with opaque skin, and the middle and bottom rows render with transparent skin in front and lateral views, respectively. The red arrows point to the increases in facial fat and posterior cervical fat.

Fig. 3 and Fig. 4 illustrate the exemplary anatomical deformation patterns of the first three principal components. Interestingly, both the male and female atlases exhibit similar deformation patterns. As shown in Fig. 3, the principal component (PC1) of the female atlas and the PC3 of the male atlas correspond to the variation in fat quantity. When a_1 of the female atlas or a_3 of the male atlas increases, the faces of both atlases get fatter (as shown in the skin-opaque view), while the facial fat and posterior cervical fat become thicker (observed in the skin-transparent view).

Fig. 4 displays the variations in head shape. As shown in Fig. 4(a), mode 2 of both genders corresponds to the changes in head length and facial proportion. When a_2 gets larger, the overall face length increases, but the forehead height decreases, indicating that the increase in overall length is contributed by the lower face part. For the female atlas,

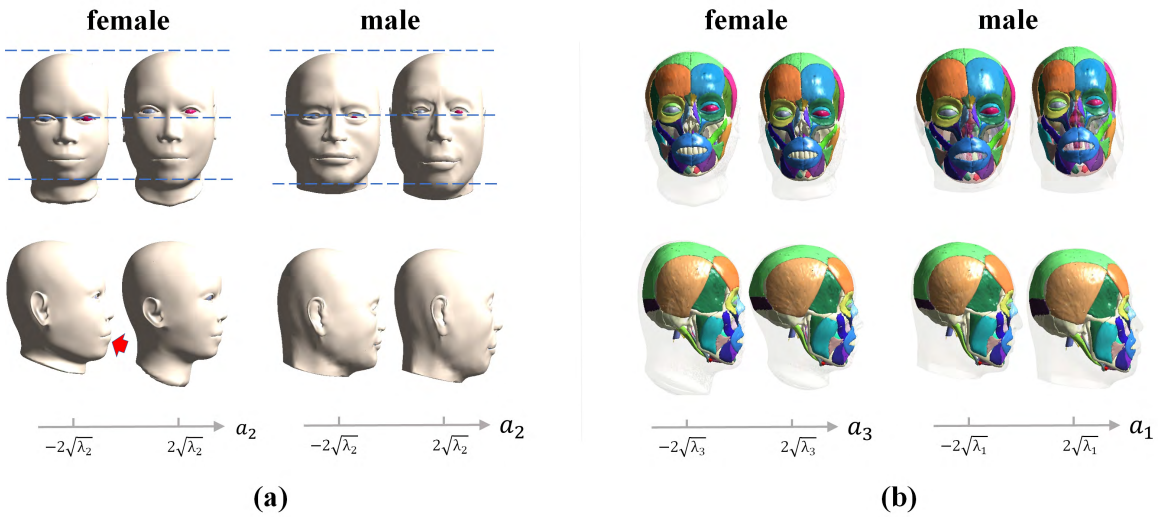

FIGURE 4. Variation modes related to head shape variations. (a). Head length and facial proportional variations. The blue lines in the front view illustrate the facial proportion differences, and the red arrow in the lateral view points to the female facial protrusion. (b). Neurocranium shape variations.

mode 2 also corresponds to the degree of facial protrusion (as pointed by the arrow in lateral view of Fig.4(a), although this variation is not obvious in the male atlas. Fig. 4(b) exhibits the shape variation of the neurocranium part. As a_3 of the female atlas or a_1 of the male atlas grows, the width of the neurocranium part decreases (as observed in the front view), while the lateral scale increases (seen from the lateral view).

B. COMPARISON WITH CHINESE POPULATION MORPHOMETRY STATISTICS

Since the DHAs are built to model the population variations, it is important to evaluate how well the atlases match with the morphometry parameters of large population statistics. We compare the somatometry and osteometry measurements of the atlases with the corresponding values of the Chinese population [43]–[45] based on over 3,500 Chinese autopsies (age>20) collected during 1950 and 2008. Somatometry and osteometry are anatomical morphometry metrics measuring the distances between the landmarks on the skin and skull, respectively. The collected somatometry data contain mean values and the standard deviations of the population, but the osteometry data contain only the mean values. Therefore, we used the z-score to measure the somatometry deviation of the atlas from the population.

$$z = (x - \mu)/\sigma \tag{2}$$

and use the r-ratio to measure the osteometry deviation of the atlas from the population:

$$r = (x - \mu)/\mu \tag{3}$$

where x is the organ mass of the atlas, μ is the mean of the population and σ is the standard deviation of the population.

We vary the shape parameter a_i of each mode within the range $[-2\sqrt{\lambda_i}, 2\sqrt{\lambda_i}]$, $(i = 1, 2, 3)$, and compute the corresponding r-ratio and z-score ranges. The results are plotted in Fig. 5. For figure clarity, we only plot the first three PCs, which account for 43.60% and 49.98% of the total variations in males and females, respectively. The names of the somatometry and osteometry parameters are represented using the Martin coding as listed in Table 3. We refer the readers to [43] for detailed definitions of these measurements. To measure the somatometry and osteometry parameters from the atlas, the skin and skull landmarks are manually specified on the atlas mesh, and then the distances between the landmarks are calculated as defined in [43].

Fig. 5 shows that the osteometric measurements of the atlases have r-scores within the range of [-0.2, 0.2], and more than half of them fall in the range of [-0.1, 0.1], meaning that the deviation of the atlas from the population mean is less than 10% of the population mean. As shown in Fig. 5, the ranges of most somatometric measurements have z-scores within [-1.96, 1.96]. If a normal distribution of the population is assumed, a z-score within [-1.96, 1.96] means the probability that the atlas parameters belonging to the population distribution is over 95%. The results reveal a reasonable agreement

TABLE 3. List of the martin coding of the osteometry and somatometry used in Fig. 5.

Organ System Osteometry Measurements	Numbers of Parts Somatometry Measurements
Maximum Cranial Length (M1)	Maximum Head Length (M1)
Basis Length (M5)	Maximum Head Breadth (M3)
Foramen Magnum Length (M7)	Minimum Frontal Breadth (M4)
Maximum Cranial Breadth (M8)	Face Breadth (M6)
Basis-Bregma Height (M17)	Bigonial Breadth (M8)
Facial Profile Length (M40)	Interpupillary Distance (M12)
Facial Breadth (M45)	Nose Breadth (M13)
Upper Facial Height (M48)	Morphological Facial Height (M18)
Orbital Breadth (M51a)	
Nasal Height (M55)	

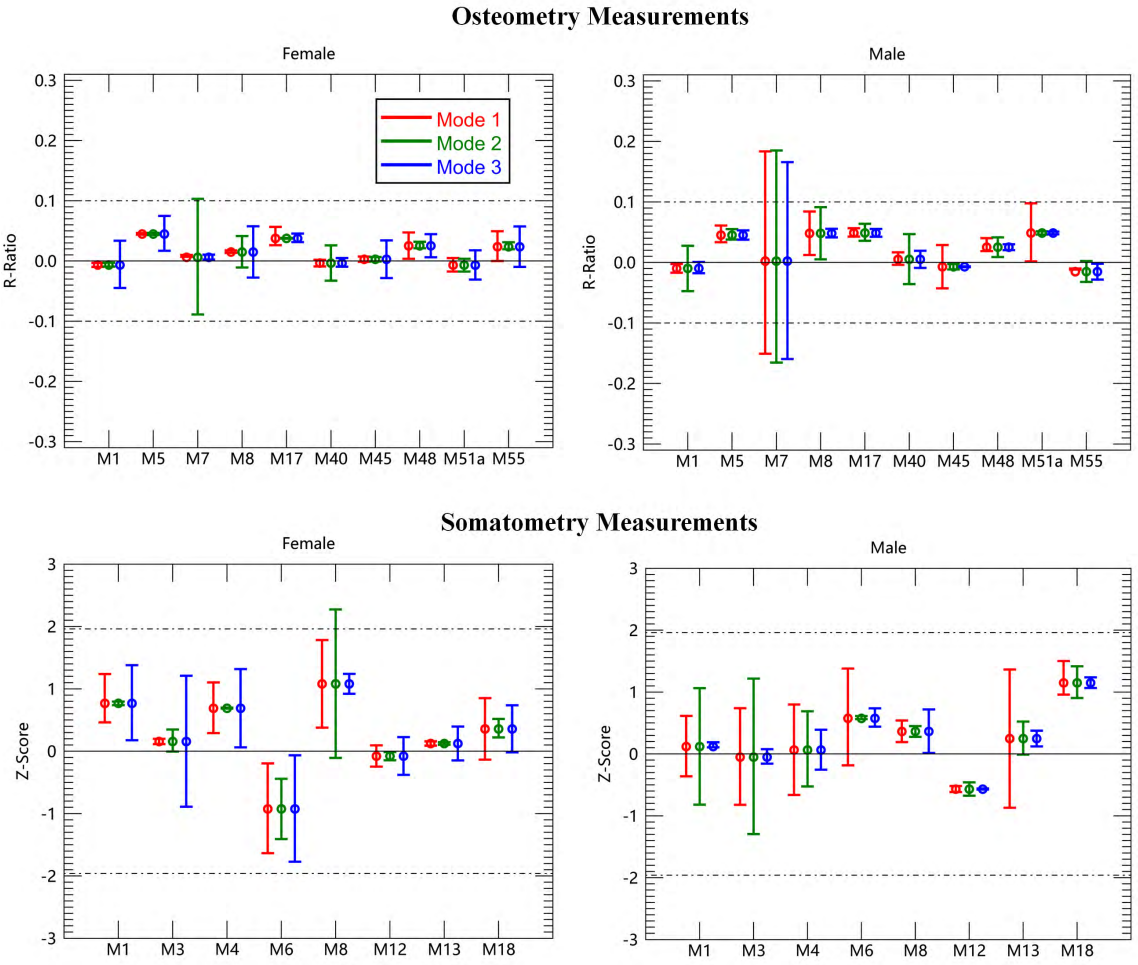

FIGURE 5. The r-ratios and z-scores comparing the atlas morphometry measurements with the population statistics of somatometry and osteometry [43]–[45]. Different variation modes are plotted with different colors. The circles mark the value of mean shape ($a_i = 0$), and error bars correspond to the range of $a_i[-2\sqrt{\lambda_i}, 2\sqrt{\lambda_i}]$. The names of the morphometry measurements are abbreviated with Martin coding as explained in Table 3.

between the atlas and the population statistics data of Chinese adults.

C. ATLAS REGISTRATION WITH INDIVIDUAL SUBJECTS

To prove the ability of the atlas in personalized anatomy modeling, we registered the atlases to the CT images of two test subjects (including one male and one female) not in the training set. The acquisition protocol of the test CT images is the same as described in the method section. Previous to the registration, the skull, skin and facial muscles are segmented from the test CT images, using the same method described in the method section. The atlas is registered using the active shape model (ASM) approach [34], which optimizes the translation, rotation, scaling and the shape parameters of the SSM to minimize the surface distances between the transformed atlas and the segmented structures of the target images. Fig. 6 demonstrates the registered atlases overlaid on the target image. The registration results provide a reasonable estimation of the anatomical structures, which are not clearly presented in the CT (for example, the detailed brain structures). This feature is beneficial for medical applications including radiotherapy planning.

IV. DISCUSSION

This study constructed deformable atlases of the entire head based on CT images of 65 Chinese adults. Realistic inter-subject anatomical variations were determined from real human subjects, and the variation ranges of the head morphometry parameters concur with the statistical values from a large Chinese population. Contrary to the existing brain atlases, we focused on modeling the gross anatomical variations of the whole-head range. As shown by the experimental results, the atlases demonstrated anatomically meaningful deformation patterns, which have not been modeled in the existing head atlases. Moreover, most existing digital head atlases have been constructed based on Caucasian anatomy; our study models the head anatomical variations of the Chinese subjects. It is interesting to see that the atlases of both genders demonstrate similar deformation patterns, implying that the two genders share common anatomical variations.

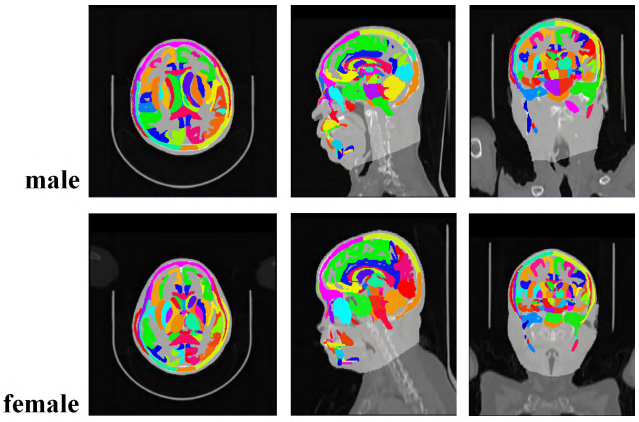

FIGURE 6. Atlas registration results of the test CT images of one male subject and one female subject. The anatomical structures of the deformed atlases are displayed as colored regions.

However, similar variation pattern may come from different principal modes of the two atlases. This is caused by the mathematical nature of PCA modeling. PCA orders the principal modes according to their variation percentages (as defined in subsection 2.4) rather than by their anatomical meaning.

The purpose of developing DHA atlases is to to provide computational tools for whole-head-level personalized simulation and medical treatment. By registering the atlases with individual CT images, the deformed atlases depict complete head anatomy, which cannot be segmented from the patient image. Due to the mesh-based atlas representation, the registration result can be easily adjusted by human experts using interactive software [46], and such adjustments are more efficient and less subjective than pure manual segmentation [47]. Therefore, the atlas registration result can provide reasonable initialization for semiautomated delineation of an organ at risk (OAR) for electromagnetic planning. Moreover, the mesh-based atlas can be readily filled into volumetric images and further converted to tetrahedral meshes for radio magnetic and biomechanics simulation. Notably, the registered atlas may not align well with the target anatomy, which is severely altered by head pathologies, because the atlas only models normal head anatomy. For these cases, the registered atlas provides a reference for the normal anatomy in contrast to the diseased anatomy.

Due to the difficulty in collecting normal subject medical images, we used only 65 training images in this study. The limited sample set may introduce a potential bias of anatomy modeling, which might account for the minor discrepancies of some morphometry parameters between our atlases and the large population statistics. Despite the limited number of training samples, the SSM learned anatomically meaningful deformation patterns of gross head anatomy. It is interesting to see that both the male and female atlases demonstrate similar deformation patterns (Fig. 3 and Fig. 4), implying that consistent anatomical variations in both genders can be learned from a relatively small sample set (46 males and 19 females). We are currently collecting more CT images, and less discrepancies between the atlas and the population statistics are expected in the near future. With enough training samples, we can even conduct comparison studies between different ages or different country regions to generate multiple deformable atlases of sub-population groups.

Another limitation regarding the training data is the use of low dose CT images. We collect health screening PET/CT images because diagnostic CT or MR images always include pathologies. However, due to the imperfect soft tissue contrast of the collected CT images, the accurate segmentation of the brain structures is not possible. To compensate for the missing anatomy in the training image, we map a reference template to each training subject as commonly performed in the image-based atlas construction studies [37], [41], [48]. However, such mapping is based on the alignment of skull, skin and facial muscles, as it does not produce faithful segmentation of the brain structures. This problem can be solved by collecting diagnostic CT or MR with minor pathological defects, which do not alter the gross head anatomy. Dual-modality CT and MR of the same patients are preferred, since they provide complementary anatomical information to each other. We are still accumulating such data to improve the accuracy of head anatomy modeling.

V. CONCLUSION

In the present study, two head deformable atlases of Chinese male and female adults were constructed based on 65 segmented CT images of healthy Chinese subjects. The statistical shape model approach was used to extract anatomically meaningful inter-subject variations. The atlases demonstrate good accuracy for anatomical morphometry modeling and personalized anatomy simulation. This study is a preliminary attempt to model inter-subject anatomical variations in the head anatomy in Chinese adults. Future improvements to the atlas can be achieved by using more training samples and more advanced shape modeling approaches. The deformable head models developed in this study will be opened to the research community in near future.

ACKNOWLEDGMENT

The author would like to thank the anonymous reviewers for their valuable comments and suggestions to significantly improve the quality of this paper.

REFERENCES

[1] J. Wang, Y. Liu, J. H. Noble, and B. M. Dawant, "Automatic selection of landmarks in T1-weighted head MRI with regression forests for image registration initialization," *J. Med. Imag.*, vol. 4, no. 4, p. 044005, 2017.
[2] A. J. Plassard, M. McHugo, S. Heckers, and B. A. Landman, "Multi-scale hippocampal parcellation improves atlas-based segmentation accuracy," *Proc. SPIE*, vol. 10133, p. 101332D, Feb. 2017.
[3] X. Yu *et al.*, "Digital human modeling and its applications: Review and future prospects," *J. X-Ray Sci. Technol.*, vol. 23, no. 3, pp. 385–400, 2015.
[4] W. Semper-Hogg, "Virtual reconstruction of midface defects using statistical shape models," *J. Cranio-Maxillofacial Surg.*, vol. 45, no. 4, pp. 461–466, 2017.
[5] X. Chen, L. Xu, Y. Sun, and C. Politis, "A review of computer-aided oral and maxillofacial surgery: Planning, simulation and navigation," *Expert Rev. Med. Devices*, vol. 13, no. 11, pp. 1043–1051, 2016.

[6] M. E. H. Wagner, J. T. Lichtenstein, M. Winkelmann, H.-O. Shin, N.-C. Gellrich, and H. Essig, "Development and first clinical application of automated virtual reconstruction of unilateral midface defects," *J. Cranio-Maxillofacial Surg.*, vol. 43, no. 8, pp. 1340–1347, 2015.

[7] J. O. Voss, V. Varjas, J.-D. Raguse, N. Thieme, R. G. Richards, and L. Kamer, "Computed tomography-based virtual fracture reduction techniques in bimandibular fractures," *J. Cranio-Maxillofacial Surg.*, vol. 44, no. 2, pp. 177–185, 2016.

[8] W. Shui, M. Zhou, Z. Wu, and Q. Deng, "An improved algorithm for craniofacial reconstruction based on landmarks registration," in *Proc. Int. Conf. Comput. Appl. Syst. Modeling (ICCASM)*, Taiyuan, China, vol. 5, Oct. 2010, pp. 498–502.

[9] W. Zhao, C. Kuo, L. Wu, D. B. Camarillo, and S. Ji, "Performance evaluation of a pre-computed brain response atlas in dummy head impacts," *Ann. Biomed. Eng.*, vol. 45, no. 10, pp. 2437–2450, 2017.

[10] Z. Yang and Z. Guo, "A three-dimensional digital atlas of the dura mater based on human head MRI," *Brain Res.*, vol. 1602, pp. 160–167, Mar. 2015.

[11] C. McIntosh, M. Welch, A. McNiven, D. A. Jaffray, and T. G. Purdie, "Fully automated treatment planning for head and neck radiotherapy using a voxel-based dose prediction and dose mimicking method," *Phys. Med. Biol.*, vol. 62, no. 15, pp. 5926–5944, 2017.

[12] F. Guerreiro *et al.*, "Evaluation of a multi-atlas CT synthesis approach for MRI-only radiotherapy treatment planning," *Phys. Med.*, vol. 35, pp. 7–17, Mar. 2017.

[13] J. Y. Lim and M. Leech, "Use of auto-segmentation in the delineation of target volumes and organs at risk in head and neck," *Acta Oncol.*, vol. 55, no. 7, pp. 799–806, 2016.

[14] C. E. Fernández-Rodríguez and A. A. A. De Salles, "On the sensitivity of the skull thickness for the SAR assessment in the intracanial tissues," in *Proc. IEEE MTT-S Latin Amer. Microw. Conf. (LAMC)*, Puerto Vallarta, Mexico, Dec. 2016, pp. 1–4.

[15] J. Wiart, *Radio-Frequency Human Exposure Assessment: From Deterministic to Stochastic Methods*. Hoboken, NJ, USA: Wiley, 2016, pp. 1–185.

[16] R. Morimoto, I. Laakso, V. De Santis, and A. Hirata, "Relationship between peak spatial-averaged specific absorption rate and peak temperature elevation in human head in frequency range of 1–30 GHz," *Phys. Med. Biol.*, vol. 61, no. 14, pp. 5406–5425, 2016.

[17] C. M. Adams and T. D. Wilson, "Virtual cerebral ventricular system: An MR-based three-dimensional computer model," *Anatomical Sci. Educ.*, vol. 4, no. 6, pp. 340–347, 2011.

[18] R. B. Trelease, "From chalkboard, slides, and paper to e-learning: How computing technologies have transformed anatomical sciences education," *Anatomical Sci. Educ.*, vol. 9, no. 6, pp. 583–602, 2016.

[19] R. L. Flores, N. Deluccia, B. H. Grayson, A. Oliker, and J. G. McCarthy, "Creating a virtual surgical atlas of craniofacial procedures: Part I. Three-dimensional digital models of craniofacial deformities," *Plastic Reconstruct. Surg.*, vol. 126, no. 6, pp. 2084–2092, 2010.

[20] R. L. Flores, N. Deluccia, A. Oliker, and J. G. McCarthy, "Creating a virtual surgical atlas of craniofacial procedures: Part II. Surgical animations," *Plastic Reconstruct. Surg.*, vol. 126, no. 6, pp. 2093–2101, 2010.

[21] S. P. Tarpada, W. D. Hsueh, S. B. Newman, and M. J. Gibber, "Formation and assessment of a novel surgical video atlas for thyroidectomy," *J. Vis. Commun. Med.*, vol. 40, no. 1, pp. 21–25, 2017.

[22] W. L. Nowinski *et al.*, "Automatic testing and assessment of neuroanatomy using a digital brain atlas: Method and development of computer- and mobile-based applications," *Anatomical Sci. Educ.*, vol. 2, no. 5, pp. 244–252, 2009.

[23] W. L. Nowinski, "3D atlas of the brain, head and neck in 2953 pieces," *Neuroinformatics*, vol. 15, no. 4, pp. 395–400, 2017.

[24] W. L. Nowinski *et al.*, "Three-dimensional stereotactic atlas of the adult human skull correlated with the brain, cranial nerves, and intracranial vasculature," *J. Neurosci. Methods*, vol. 246, pp. 65–74, May 2015.

[25] W. L. Nowinski, "Toward the holistic, reference, and extendable atlas of the human brain, head, and neck," *Brain Inform.*, vol. 2, no. 2, pp. 65–76, 2015.

[26] N. Mitsuhashi, K. Fujieda, T. Tamura, S. Kawamoto, T. Takagi, and K. Okubo, "Bodyparts3D: 3D structure database for anatomical concepts," *Nucl. Acids Res.*, vol. 37, pp. D782–D785, Jan. 2009.

[27] E. G. Lee *et al.*, "Investigational effect of brain-scalp distance on the efficacy of transcranial magnetic stimulation treatment in depression," *IEEE Trans. Magn.*, vol. 52, no. 7, Jul. 2016, Art. no. 5000804.

[28] C. I. Bargmann and W. T. Newsome, "The brain research through advancing innovative neurotechnologies (brain) initiative and neurology," *JAMA Neurol.*, vol. 71, no. 6, pp. 675–676, 2014.

[29] T. R. Insel, S. C. Landis, and F. S. Collins, "The NIH BRAIN initiative," *Science*, vol. 340, no. 6133, pp. 687–688, 2013.

[30] G. M. Shepherd *et al.*, "The human brain project: Neuroinformatics tools for integrating, searching and modeling multidisciplinary neuroscience data," *Trends Neurosci.*, vol. 21, no. 11, pp. 460–468, 1998.

[31] D. C. Van Essen *et al.*, "The human connectome project: A data acquisition perspective," *Neuroimage*, vol. 62, no. 4, pp. 2222–2231, 2012.

[32] A. R. Jones, C. C. Overly, and S. M. Sunkin, "The Allen brain atlas: 5 years and beyond," *Nature Rev. Neurosci.*, vol. 10, no. 11, p. 821–828, 2009.

[33] L. Fan *et al.*, "The human brainnetome atlas: A new brain atlas based on connectional architecture," *Cerebral Cortex*, vol. 26, no. 8, pp. 3508–3526, 2016.

[34] T. Heimann and H.-P. Meinzer, "Statistical shape models for 3D medical image segmentation: A review," *Med. Image Anal.*, vol. 13, no. 4, pp. 543–563, 2009.

[35] H. Wang, X. Sun, L. Huo, X. Tang, and C. Liu, "Construction of deformable trunk atlas of Chinese human based on multiple PET/CT images: Preliminary results," in *Digital Human Modeling. Applications in Health, Safety, Ergonomics, and Risk Management: Ergonomics and Design*, V. G. Duffy, Ed. Cham, Switzerland: Springer, 2011, pp. 69–77.

[36] H. Wang, D. B. Stout, and A. F. Chatziioannou, "Estimation of mouse organ locations through registration of a statistical mouse atlas with micro-CT images," *IEEE Trans. Med. Imag.*, vol. 31, no. 1, pp. 88–102, Jan. 2012.

[37] H. Wang, D. B. Stout, and A. F. Chatziioannou, "A deformable atlas of the laboratory mouse," *Mol. Imag. Biol. MIB, Pub. Acad. Mol. Imag.*, vol. 17, no. 1, pp. 18–28, Feb. 2015.

[38] I. Wolf *et al.*, "The medical imaging interaction toolkit," *Med. Image Anal.*, vol. 9, no. 6, pp. 594–604, 2005.

[39] W. E. Lorensen and H. E. Cline, "Marching cubes: A high resolution 3D surface construction algorithm," *ACM SIGGRAPH Comput. Graph.*, vol. 21, no. 4, pp. 163–169, 1987.

[40] Turbosquid. *Male and Female Anatomy Complete Pack (Textured)*. Accessed: Apr. 4, 2018. [Online]. Available: https://www.turbosquid.com/3d-models/male-female-anatomy-body-3d-max/602826/

[41] H. Wang *et al.*, "Deformable torso phantoms of Chinese adults for personalized anatomy modelling," *J. Anatomy*, vol. 233, no. 1, pp. 121–134, 2018.

[42] F. L. Bookstein, "Landmark methods for forms without landmarks: Morphometrics of group differences in outline shape," *Med. Image Anal.*, vol. 1, no. 3, pp. 225–243, 1997.

[43] X. Shao, *Anthropometric Handbook*. Mainland, China: Shanghai Lexicographical Publishing House, 1985, pp. 377–428.

[44] L. Du, "The measurement and analysis of Chinese han human head-face dimensions," M.S. thesis, Huazhong Univ. Sci. Technol., Wuhan, China, 2008.

[45] L.-L. Du, Y.-J. Lan, H.-J. Wang, L.-M. Wang, Z.-L. Wang, and W.-H. Chen, "Analysis of craniofacial characteristics of Han nationality," *Ind. Health Occupational Diseases*, vol. 36, no. 1, pp. 11–15, 2010.

[46] W. Valenzuela *et al.*, "FISICO: Fast image segmentation correction," *PLoS ONE*, vol. 11, no. 5, p. e0156035, 2016.

[47] C.-J. Tao *et al.*, "Multi-subject atlas-based auto-segmentation reduces interobserver variation and improves dosimetric parameter consistency for organs at risk in nasopharyngeal carcinoma: A multi-institution clinical study," *Radiotherapy Oncol.*, vol. 115, no. 3, pp. 407–411, 2015.

[48] W. P. Segars *et al.*, "Population of anatomically variable 4D XCAT adult phantoms for imaging research and optimization," *Med. Phys.*, vol. 40, no. 4, p. 043701, 2013.

ZHAOFENG CHEN received the B.Eng. degree in information engineering from the Xi'an Institute of Communication, Xi'an, China, in 2004, and the M.S. degree in electronics and communication engineering from the Dalian University of Technology, Dalian, China, in 2010, where he is currently pursuing the Ph.D. degree with the Faculty of Electronic Information and Electrical Engineering. His current research interests include medical image processing and machine learning.

TIANSHUANG QIU received the B.Eng. degree in electrical engineering from Tianjin University, Tianjin, China, in 1983, the M.S. degree in electrical engineering from the Dalian University of Technology, Dalian, China, in 1993, and the Ph.D. degree in electrical engineering from Southeastern University, Nanjing, China, in 1996. He was a Post-Doctoral Fellow with the Department of Electrical Engineering, Northern Illinois University, USA, from 1996 to 2000. He is currently a Professor with the Faculty of Electronic Information and Electrical Engineering, Dalian University of Technology. His research interests include medical image processing and signal processing.

LI HUO received the M.S. degree in nuclear medicine from Peking University, Beijing, China, in 2001, and the Ph.D. degree in nuclear medicine from Tsinghua University, Beijing, in 2007. She is currently a Professor with the Department of Nuclear Medicine, Peking Union Medical College Hospital, Beijing. Her research interests include nuclear medicine and medical image processing.

LIJUAN YU received the B.Eng. degree in clinical medicine and the M.S. degree in diagnostic radiology from Harbin Medical University, Harbin, China, in 1988 and 1993, respectively, and the Ph.D. degree in medical imaging from Guangzhou First Military Medical University, Guangzhou, China, in 2004. She is currently a Professor with the Affiliated Cancer Hospital, Hainan Medical University, Haikou, China. Her research interests include nuclear medicine and medical image processing.

HONGCHENG SHI received the B.Eng. degree in imaging medicine from Soochow University, Suzhou, Zhejiang, China, in 1991, and the Ph.D. degree in imaging and nuclear medicine from Fudan University, Shanghai, China, in 2001. He is currently a Professor with the Department of Nuclear Medicine, Zhongshan Hospital, Fudan University. His research interests include nuclear medicine and medical image processing.

YANJUN ZHANG received the B.Eng. degree in imaging medicine from Dalian Medical University, Dalian, China, in 1983. He is currently a Professor with the Department of Nuclear Medicine, The First Affiliated Hospital of Dalian Medical University, Dalian. His research interests include nuclear medicine and medical image processing.

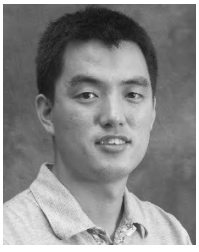

HONGKAI WANG received the B.Eng. degree in electronic information engineering from Beihang University, Beijing, China, in 2003, and the Ph.D. degree in biomedical engineering from Tsinghua University, Beijing, in 2009. From 2009 to 2011, he was a Post-Doctoral Fellow with the University of California, Los Angeles, CA, USA, where he was a Senior Researcher from 2011 to 2014. He is currently an Associate Professor with the Faculty of Electronic Information and Electrical Engineering, Dalian University of Technology. His research interests include medical image processing and biomedical engineering.